



Universiteit  
Leiden  
The Netherlands

## Microfluidic 3D cell culture for high throughput screening

Trietsch, S.J.

### Citation

Trietsch, S. J. (2017, December 18). *Microfluidic 3D cell culture for high throughput screening*. Retrieved from <https://hdl.handle.net/1887/57795>

Version: Not Applicable (or Unknown)

License: [Licence agreement concerning inclusion of doctoral thesis in the Institutional Repository of the University of Leiden](#)

Downloaded from: <https://hdl.handle.net/1887/57795>

**Note:** To cite this publication please use the final published version (if applicable).

Cover Page



Universiteit Leiden



The handle <http://hdl.handle.net/1887/57795> holds various files of this Leiden University dissertation

**Author:** Trietsch S.J.

**Title:** Microfluidic 3D cell culture for high throughput screening

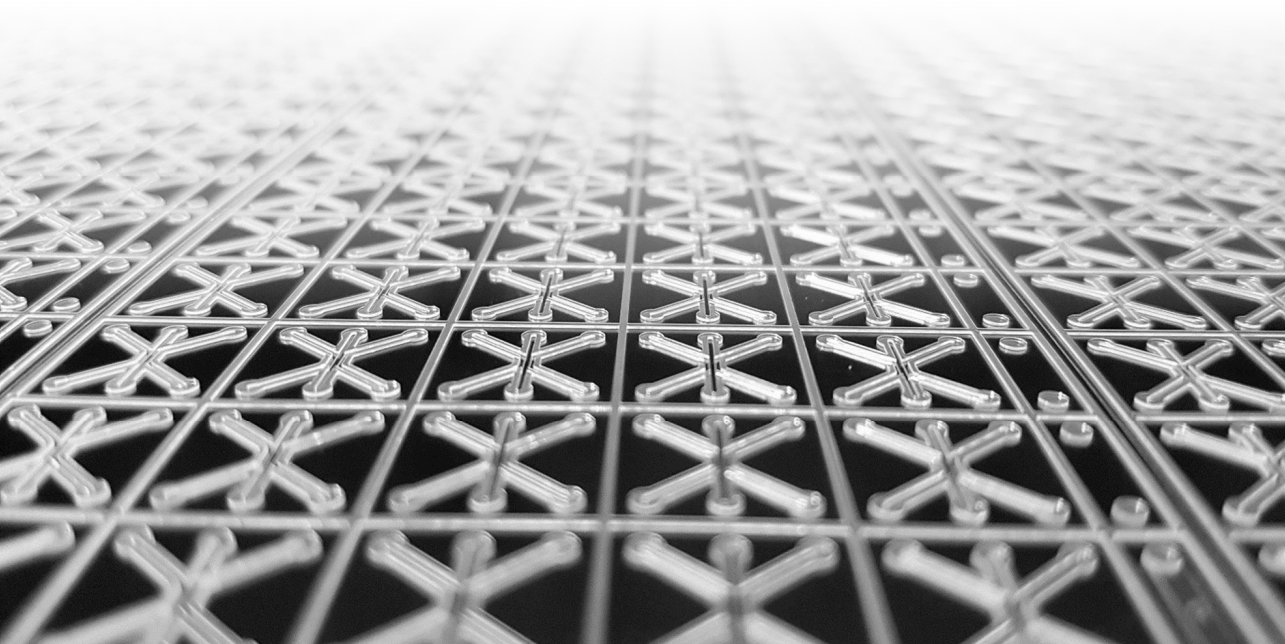
**Date:** 2017-12-18

## Chapter 4

# Microfluidic titer plate for stratified 3D cell culture

SJ Trietsch, GD Israëls, J Joore, T Hankemeier, P Vulto

Lab on a Chip





## Abstract

Human tissues and organs are inherently heterogeneous. Their functionality is determined by the interplay between different cell types, their secondary architecture, vascular system and gradients of signaling molecules and metabolites. Here we propose a stratified 3D cell culture platform, in which adjacent lanes of gels and liquids are patterned by phaseguides to capture this tissue heterogeneity. We demonstrate 3D cell culture of HepG2 hepatocytes under continuous perfusion, a rifampicin toxicity assay and co-culture with fibroblasts. 4T1 breast cancer cells are used to demonstrate invasion and aggregation models. The platform is incorporated in a microtiter plate format that renders it fully compatible with automation and high-content screening equipment. The extended functionality, ease of handling and full compatibility to standard equipment is an important step towards adoption of Organ-on-a-Chip technology for screening in an industrial setting.

4

## Introduction

There is a great need for more predictive *in vitro* screening models for early de-risking in drug discovery and development. A trend towards better mimicry of the *in vivo* microenvironment is to culture relevant tissues in three dimensions instead of conventional monolayers.<sup>1</sup> Cells are suspended in a surrogate extracellular matrix (ECM), which results in more natural morphology and has a tremendous effect on gene expression, metabolism and ultimately drug efficacy<sup>2</sup> and toxicology.<sup>3,4</sup>

Efforts are ongoing to add further organotypic functionality to these 3D cell cultures by considering the structural, mechanical and chemical complexity of tissues. With roots in the fields of tissue engineering and lab-on-a-chip, “Organs-on-Chips”<sup>5</sup> aim to exploit the precise control of liquids in the microfluidic space to control the tissue microenvironment.

Over the past years, a wide variety of mono and co-culture<sup>6</sup> models have been developed including liver,<sup>7–11</sup> kidney,<sup>12,13</sup> colon,<sup>14,15</sup> lung,<sup>16,17</sup> cornea,<sup>18</sup> heart,<sup>19</sup> breast,<sup>20,21</sup> neuronal,<sup>22,23</sup> and vascular models.<sup>24</sup> Different models have been combined to achieve multi-organ integration<sup>25–27</sup> and have been adapted to disease specific models.<sup>28–30</sup>

The essence of improving translatability of *in vitro* models is to capture the complexity of heterogeneous tissues. This includes perfusion flow aspects, co-culture flexibility and communication between various distinct microenvironments. Today's preferred method to achieve heterogeneous tissue complexity is by compartmentalization of the microfluidic space using physical separations. Compartmentalization techniques reported include usage of membranes,<sup>31,32</sup> valves,<sup>33</sup> tightly placed pillars,<sup>10</sup> long narrow channels,<sup>34</sup> or other tight gaps.<sup>35</sup> However compartmentalization can severely hamper communication, because of long diffusion distances or prevention of direct cell–cell interactions.

Here we propose a stratified 3D cell-culture platform in which tissues and perfusion lanes are patterned adjacently, without physical separation. We employ a two- and three-lane bioreactor in which lanes are separated by phaseguides. As described previously,<sup>36–39</sup> phaseguides are geometric features that act as pressure barriers due to meniscus pinning. One or more lanes are filled with gel-embedded cells. Remaining lanes are employed for a perfusion flow, a challenge compound or staining reagents. Perfusion by leveling of reservoirs supplies nutrients, oxygen and removes waste metabolites. Co-cultures enable studying cell–cell interaction and construction of complex tissues.

Here we present a proof of concept by culturing HepG2 liver cells in 3D under continuous perfusion. The cells exhibit excellent survival, and are used for hepatotoxicity assessment of rifampicin. Mixed and side-by-side cultures of hepatocytes and fibroblasts demonstrate co-culture flexibility of the system. Invasion and aggregation of tumor cells demonstrates migration assay capabilities. Arrays of 40 or 96 microchambers are embedded in a microtiter-based screening plate that is pipette-operatable and fully compatible with industrial readout and liquid handling equipment. The phaseguide-stratified 3D culture platform provides a complete toolbox for modeling tissues of arbitrary complexity. It is among the most elegant approaches for constructing complex heterogeneous tissues and Organ-on-a-Chip models.

## Materials & methods

### Chips fabrication

Microfluidic chips were fabricated using a dry film resist (DFR) based process as extensively described previously.<sup>40–43</sup> Briefly, a 30  $\mu\text{m}$  thick permanent dry film resist (Ordyl SY330, Elga Europe, Italy) was hot laminated on 175  $\mu\text{m}$  thick glass substrates and exposed using a Karl Suss MA45 mask aligner through a transparency foil mask of the phaseguides printed on an AGFA Accuset 1500 photo plotter at 3000 dpi. Three additional layers were laminated on top and exposed with a second mask in order to pattern microfluidic channel walls. After post baking, the chips were developed using BMR developer (Elga Europe, Italy). Chips were capped with a glass substrate with predrilled access holes in a hot press (5 min, 95°C, 60 N  $\text{cm}^{-2}$ ), resulting in 120  $\mu\text{m}$  high microfluidic chambers with 30  $\mu\text{m}$  high phaseguides. Bottomless 384-wells plates were glued on top of the inlets using non-cytotoxic medical grade glue (Loctite M-31 CL, Henkel, Germany).

### Cell culture

HepG2 and 4T1 cells were cultured in Dulbecco's Modified Eagle Medium (DMEM) supplemented with 10% fetal calf serum (FCS), 50 U  $\text{mL}^{-1}$  Penicillin and 50 mg  $\text{mL}^{-1}$  Streptomycin (P/S) and stable glutamine (PAA Laboratories GmbH, Cölbe, Germany). 3T3 cells were cultured in DMEM/ FCS/P/S with added stable glutamine, both wild type and transfected with mCherry-LifeAct. Unless otherwise specified all cell culture reagents were acquired from Life Technologies, Carlsbad, CA, USA.

For 3D cell culture, cells were harvested, washed once in full medium, pelleted and resuspended in the appropriate ECM on ice. Unless stated otherwise, Matrigel was used at 9 mg  $\text{mL}^{-1}$  concentration (BD Matrigel, lot 2152611 and 23060, BD Bioscience, Franklin Lakes, NJ USA). Type I collagen (rat tail) was neutralized with  $\text{Na}_2\text{CO}_3$  (Alfa Aesar, Karlsruhe, Germany) buffered with 100 mM HEPES and diluted to 3 mg/mL using medium, before resuspending cells. Unless otherwise specified, cells were resuspended at  $2.5 \cdot 10^7$  cells  $\text{mL}^{-1}$ . For mixed co-culture, HepG2 and 3T3 cells were mixed in a 4 : 1 ratio for a total cell count of  $2.5 \cdot 10^7$  cells  $\text{mL}^{-1}$ .

## Plate loading

The gel with cells is patterned adjacent to one or two flanking empty lanes. Cells suspended in liquid ECM were loaded into the microfluidic chips, where it is sucked into the phaseguide defined space by capillary force. After gelation (10 min at 37°C), the flanking lanes are filled with media, which can either be static or passively perfused by leveling of two connected wells. Due to the hydrodynamic resistance of the small connecting channels between the wells and the culture chamber, an average fluid flow of  $1.5 \mu\text{L h}^{-1}$  is achieved, allowing for 24 h of perfusion with 100  $\mu\text{L}$  of medium. In most cases media was exchanged three times per week for convenience reasons.

## Assays

For toxicity assays, rifampicin was dissolved in DMSO and diluted in the perfusion media resulting in medium with 0.5% DMSO and varying rifampicin concentrations up to 640 mM. Live/dead assays were performed by washing the culture chamber twice with PBS before incubating for 30 min with 2  $\mu\text{M}$  calcein AM and 4  $\mu\text{M}$  ethidium homodimer-1 in phenol red and serum free medium (Invitrogen L3224 LIVE/DEAD1 Viability/Cytotoxicity Kit for mammalian cells, Life Technologies, USA). The stained cells were imaged using an Olympus IX81 inverted fluorescence microscope with automated stage and analyzed using CellM and ImageJ (Fiji) software. Confocal images were obtained using a Leica SP5 confocal microscope and analyzed using LAS-AF software and ImageJ.

## Results and discussion

### Device

Fig. 1 shows the microtiter plate setup for 3D heterogeneous cell and tissue culture. The 384 well plate has been modified on the bottom-side with microfluidic structures. Two designs have been used. The plate depicted in Fig. 1 contains 40 culture chambers, each with three inlets and three outlets that are connected to corresponding wells. A second plate is also used containing 96 culture chambers, each with two inlets and one outlet. Each chamber is 4.5 mm in length and consists of three resp. two 200  $\mu\text{m}$  wide, 120  $\mu\text{m}$  high lanes that are separated by 50  $\mu\text{m}$  wide, 30  $\mu\text{m}$  high phaseguides. A gel is patterned in one of the three lanes by simply pipetting the gel in the corresponding inlet well. The gel is sucked into the microfluidic chamber by capillary force, but the meniscus pinning effect prevents

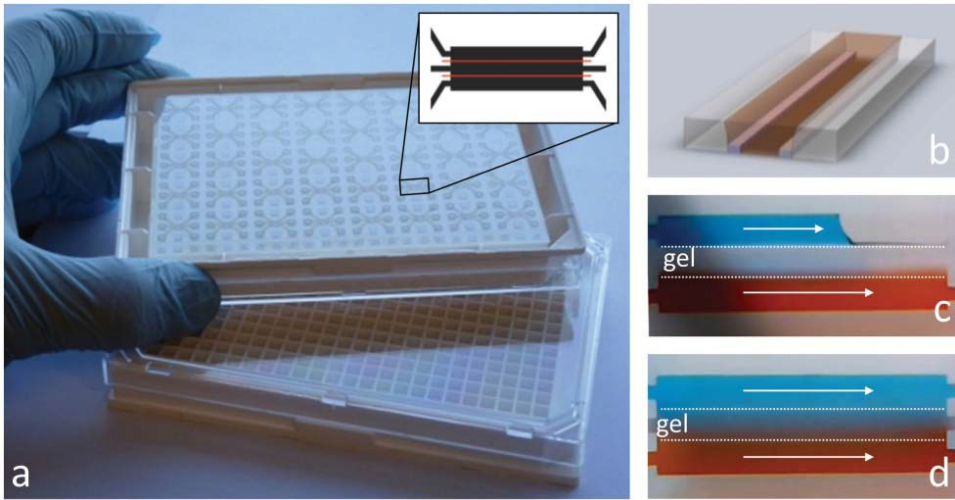


**Figure 1** | (a) 384-well format 3D cell culture plate with 40 three-lane culture chambers manufactured in the bottom plate. Inset depicts the design of a single culture chamber with phaseguide positions in red. (b) Artist impression of culture chamber with gel confined in middle lane between phaseguides, flanked by perfusion lanes. (c) Food dye being filled in flanking lanes, dotted line indicates phaseguide position. (d) Perfused media forming a gradient across gel.

the gel from overflowing into one of the flanking lanes. Upon gelation, adjacent lanes can be filled with a second gel or be used for perfusion. Since the phaseguide is merely a pinning barrier that is not higher than one fourth of the channel height, free communication between the three lanes through diffusion is maintained. This is demonstrated in Fig. 1c and d by patterning matrigel (middle lane) flanked by a red and blue food dye. The red and blue dyes are diffusing into the matrigel to form a gradient. Various gradient regimes are possible. When both lanes are perfused continuously, a constant transverse gradient is formed. Without perfusion, the gradient equilibrates over time, ultimately resulting in a homogeneous mixture.

As opposed to often-used silicone rubber (polydimethylsiloxane, PDMS) based systems, the hybrid glass–DFR system is impermeable to gasses giving complete control over gas pressure in the tissues. The plate is equipped with a thin

175  $\mu\text{m}$  bottom glass plate to ensure compatibility with imaging techniques such as phase contrast, fluorescence, confocal, and multi-photon microscopy as well as with high content screening (HCS) automated readers.

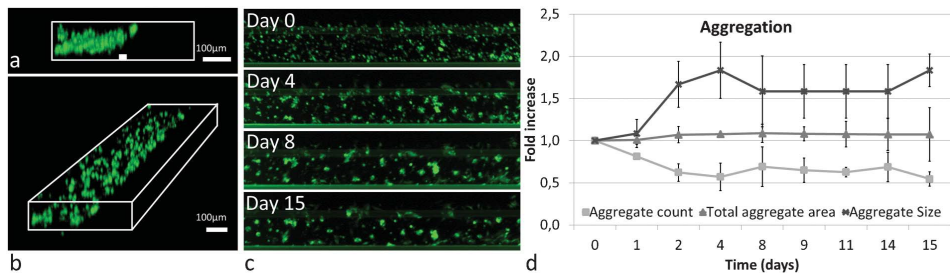


**Figure 2 |** Fluorescent HepG2 cells in an extracellular matrix gel in a two-lane microfluidic chamber: (a, b) confocal analysis of cells 48 h after seeding demonstrates a 3D distribution of cells throughout the chamber; (c) image sequence showing clustering of cells over time; (d) quantification of clustering and proliferation behavior of cells in a microfluidic 3D environment: cells aggregate into clusters, while proliferation becomes near zero.

## Perfused 3D cell culture

Fig. 2 shows GFP transfected HepG2 human hepatocytes in matrigel flanked by a perfusion flow up to 15 days in culture. Fig. 2a shows confocal image of the cell culture upon 48 h in culture. Notwithstanding the relatively shallow chamber height of 120 μm, cells and aggregates are observed throughout the microfluidic space. This indicates that sedimentation does not significantly affect the distribution of cells in the gel. Fig. 2b and c shows the behavior of cells over time. The size of aggregates increases over time, the number of aggregates decreases, but no change in the overall area of the sum of aggregates is observed. This indicates that no significant proliferation occurs in 3D, as opposed to the high proliferation in conventional 2D culture. The formation of low proliferative three-dimensional cell clusters when culturing cells embedded in surrogate extracellular matrices is well documented in

literature. The clustering is associated as a first step in the process towards a more metabolic competent model.<sup>44–46</sup> After 7 days the number and size of clusters stabilized. The clusters maintained near complete viability as confirmed by fluorescent live/dead staining.

As a proof of principle for a toxicity assay, hepatotoxicity of rifampicin was assayed. HepG2 cells were perfused with varying concentrations of up to 640 μM rifampicin for 48 and 96 h and at least three replicates were assayed for viability using a fluorescent live/dead stain at day 7 after seeding. Fig. 3a shows a series of images

of cells exposed to different doses of rifampicin, acquired using automated microscopy on a single plate. Viability of the cell clusters was scored and normalized to the number of clusters. Fig. 3b shows the dose response curve for viability of clustered hepatocytes upon rifampicin exposure. The results demonstrate the expected dose-dependent cell death, increasing with dose and exposure time.

Conventional 2D cell cultures need to be passaged up to several times a week in order to maintain viability, often requiring harsh treatments like trypsinization and scraping. 3D cell cultures under perfusion form stable tissues that show full viability for several weeks, circumventing the need to passage. The perfusion flow provides nutrients and oxygen and removes waste metabolites. This yields stable culture conditions, whereas conventional static culture systems often undergo cycles of acidification, nutrient depletion, waste build-up and evaporation. In the results of Fig. 2, however, media were exchanged three times a week for convenience reasons, resulting in perfusion for approximately half of the time before liquid levels equalized. Nonetheless we observed no significant effect on the stability of the cell culture. The reason may be that effects are limited by the presence of a relatively large volume of media in the connected wells that can act as a source and sink for nutrients and metabolites in the microchamber. Clearly in a future design, perfusion times will be extended by increasing the hydrodynamic resistance of the channels.

The gel lane has a width of 200  $\mu\text{m}$ , reflecting the physiological distance between two capillary vessels in a human body. The gel matrix protects cells from shear stress generated by the perfusion flow. In contrast to non-gel based perfusion systems, the gel matrix limits rapid efflux of signaling molecules and thus maintains a biologically relevant microenvironment.

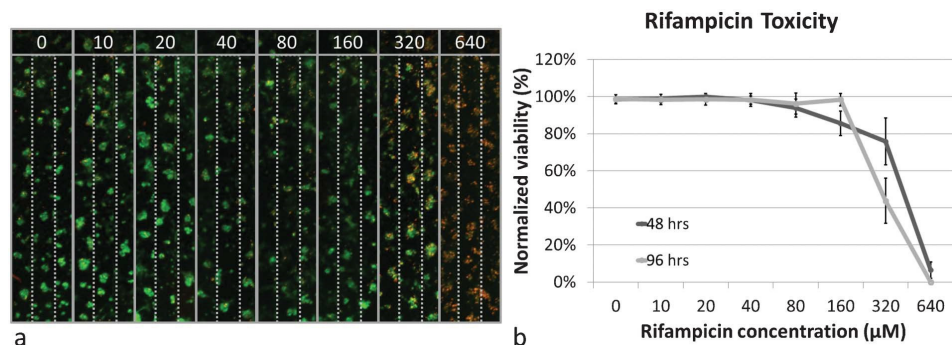


**Figure 3** | (a) Image array of one-week old HepG2 spheroids exposed to varying concentrations of rifampicin for 96 h, followed by fluorescent live/dead staining (green/red); (b) dose response curve of rifampicin toxicity upon 48 and 96 h of exposure.

The image stack of Fig. 3a was acquired by automated fluorescence microscopy of one single plate containing 96 microchambers. Due to the shallow chamber height, all cells and clusters are sufficient in focus for quantification. The fact that standard 2D imaging techniques can be applied to 3D cultures in these shallow culture chambers offers an excellent balance between superior 3D functionality and the ease of imaging associated with 2D cultures.

The above results convincingly demonstrate that the microfluidic plates presented here are fully compatible with advanced imaging techniques such as confocal, phase contrast, and fluorescent imaging. This is largely facilitated by the thin 175  $\mu\text{m}$  bottom glass. Fluorescent and phase contrast images were acquired by automated microscopy, demonstrating compatibility of the titer-plate based microfluidic platform with high content screening (HCS) assays.

### Co-culture and cell migration

The three-lane reactor setup facilitates different types of co-cultures, including cells mixed in the same ECM (mixed co-culture), different cell types patterned in adjacent lanes (adjacent co-culture) and different cell types patterned in lanes that are not in direct contact but communicate, e.g. through a perfusion flow or third gel (separated co-cultures). Fig. 4a–c illustrates these different co-culture methods. To demonstrate co-culture functionality of the plate, HepG2 hepatocytes were co-cultured with 3T3 fibroblasts cells in both mixed and adjacent modes (see Fig. 4d, e). The two co-cultures with fibroblasts result in very different tissue types. In the mixed mode, dense aggregates of fibroblasts and hepatocytes are formed. No

significant change in hepatocyte morphology is observed in adjacent cell culture. As supported by fibril formation observed in 3T3 mono-culture, the aggregates in the mixed co-culture are thought to be formed by fibroblasts that mechanically contract and support hepatocytes. The absence of any contraction of the hepatocytes in adjacent co-culture illustrates the ability to distinguish between changes in morphology by excreted signaling molecules and direct cell–cell interaction. Comparison of adjacent and separated co-cultures could be used to distinguish between local (paracrine) signaling and long distance (endocrine) cell–cell communication. An example of an endocrine system would be a liver–kidney co-culture or a liver–heart co-culture. Such cultures can for example be used to study liver mediated nephro- or cardiotoxicity.

Here we describe devices with two or three lanes, but it is clear that an arbitrary number of lanes can be patterned in order to increase the level of complexity of the model. One could try to capture the secondary architecture of an organ up to the level of a “living coupe”; a carefully designed architecture of lanes containing cell types and perfusion sites behaving like a section of an organ in a living organism.

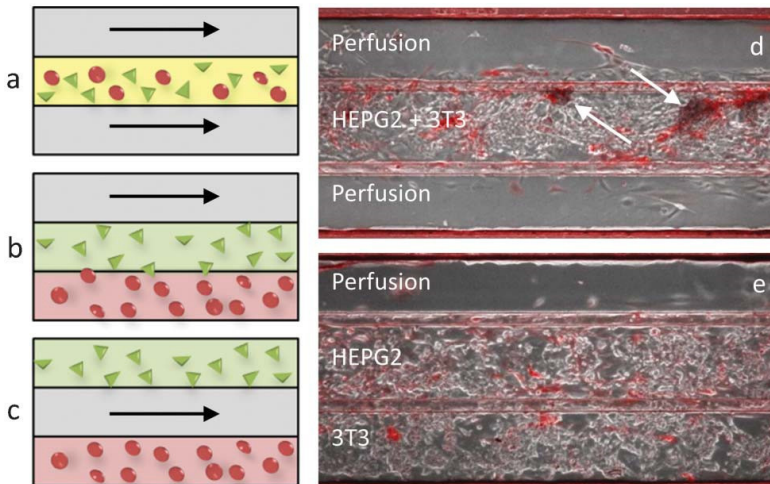


**Figure 4** | Schematic representation of (a) mixed co-culture, (b) adjacent co-culture, (c) separate co-culture configurations with perfusion through empty lanes. (d) Mixed and (e) adjacent co-culture of HepG2 hepatocytes and 3T3 mCherry fibroblasts, with mixed co-culture resulting in tighter aggregates as indicated by

## Contraction and invasion

The potential of the platform to support migration assays was investigated using 4T1 breast cancer cells cultured in collagen (Collagen 1, rat tail). A 4T1 cell loaded collagen gel was patterned adjacent to a clean collagen lane. Invasion of the 4T1 cells into the adjacent lane was monitored using time lapse imaging. Initial contraction towards the empty collagen lane caused formation of a boundary, followed by invasion into the empty collagen lane. Fig. 5 depicts this invasion process as quantified by the area of the middle lane that is covered by invaded cells. Additionally, 4T1 cells in a single lane showed strong contraction (see Fig. S1, ESI3). Within 48 h dense aggregates are formed and in prolonged cultures, cells grow out of these aggregates that ultimately disintegrate. In single-lane collagen gels, centric aggregation into spheroids was observed. Such spheroids can become very dense showing increased cell death in the center of the spheroid. This effect indicates that even on this scale necrotic core formation might be induced by hampered nutrient diffusion, resulting in an interesting model for tumor formation and angiogenesis. Examples of practical applications are wound healing-, chemotaxis- and invasion assays. In combination with the above described co-culture and gradient flexibility, a range of invasion assays can be designed under precisely controlled conditions.

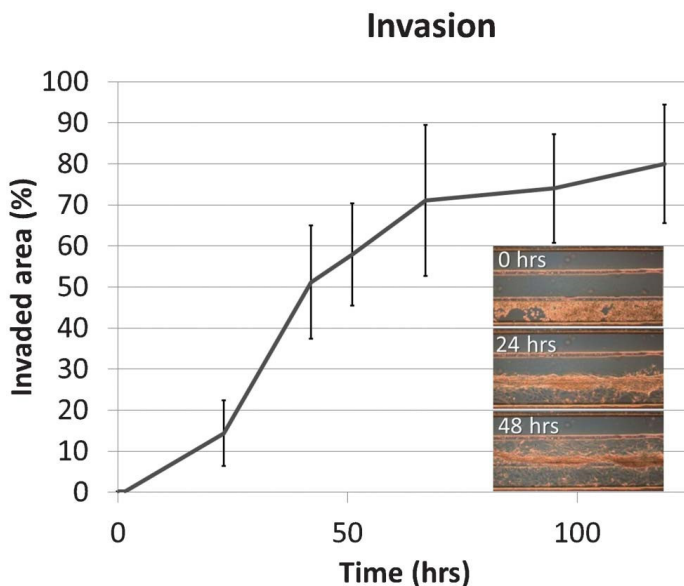


**Figure 5 |** 4T1 cells cultured in collagen I next to a cell free collagen lane are invading into the adjacent lane. Invasion was quantified as the area of the central lane covered with invaded cells

## **Organ-on-a-Chip: bridging the technology acceptance gap**

In the section above we introduced a platform technology for heterogeneous tissue modeling in a 3D configuration. We expect that the stratified culture approach using phaseguides will provide the basis for a range of culture models implemented by ourselves and others and ultimately become available for the pharmaceutical industry and the clinic. The success of the platform greatly depends on whether the technology acceptance gap is efficiently bridged. Both Lab-on-a-Chip technology and 3D cell culture have been around since the early 1990's. Although there is a clear trend towards acceptance by the pharmaceutical industry, their uptake is still limited. Clearly improved performance over current technologies, unique capabilities and/or reduced costs will ultimately drive acceptance, provided these advantages outweigh the cost of implementing a new technology (Table 1). Prerequisites include a good ease of use, low initial investments and the availability of well documented, fully validated applications.

During the design of the platform presented in this paper, we have paid careful consideration to address these aspects. The platform offers improved performance with respect to standard cell culture due to the well-documented and proven superiority of 3D cell cultures. In addition, the system boasts capabilities that are hardly available in modern cell culture, including continuous perfusion, co-culture capabilities and gradient functionalities, all aspects are fully scalable in throughput due to the microtiter plate footprint. An inherent benefit of miniaturization is the reduced consumption of reagents, which significantly reduces costs or enables screening of more data points. For example, ECM matrix preparations and cell material can be extremely costly and/or scarce, especially when working with primary cells or stem cell derived cells.

The platform offers ease of use comparable to conventional microtiter plates, as it is fully pipette-operated and can be used with standard readout equipment. The microtiter plate format reduces initial investment to near-zero as it renders the system fully robot and HCS equipment compatible, thus alleviating the need for customized equipment. A point of attention remains full validation of the system. Efforts are on-going for implementation and full validation of a range of tissue models against both state-of-the-art assays, as well as retrospective and ultimately prospective clinical validation studies. The ultimate goal is to provide a better alternative to both animal testing as well as conventional cell culture techniques.

Table 1 Overview of incentives and prerequisites required to bridge the technology acceptance gap

Incentives	Projection on phaseguide-stratified approach
Improved performance:	Better predictive data points through 3DECM embedment
Unique capabilities:	Full co-culture capabilities, perfusion flow, gradients
Cost reduction:	Reduced reagent consumption (gel, cells, compounds) Increased numbers of data points
Prerequisites	
Ease of use:	Pipette operation, passive perfusion, standard readout
Low initial investment:	No external equipment required, fully compatible with robot handling and HCS readouts.
Validation:	Full validation for a range of tissue models is ongoing

## Conclusion

In this paper, we introduce a novel platform for organ and tissue-on-a-chip culture of deliberate complexity. The platform employs phaseguides to pattern lanes with gels and liquids in a stratified manner. We demonstrate the functionality of the platform for 3D cell culture under continuous perfusion, co-culture and invasion. The microtiter-plate format is shown to be compatible with fluorescent assays as well as confocal and automated microscopy. As such, phaseguide-stratified 3D tissue culture makes Organ-on-a-Chip technologies amenable to screening in an industrial setting.

## Acknowledgements

We thank Prof. Dr Hans Tanke for the use of the imaging facilities at the Department of Molecular Cell Biology, Leiden University Medical Center. We thank Rafael Zwier and Martijn Witlox of the Fine Mechanical Department of the Faculty of Science of Leiden University as well as Dr Athanasios T. Giannitsis for their assistance in chip fabrication. We thank Dr Sandrine L. Ellero for valuable discussions on cell biology and assay development. This work is (co)financed by Technologiestichting STW and the Netherlands Metabolomics Centre (NMC) which is a part of The Netherlands Genomics Initiative/Netherlands Organization for Scientific Research.

## References

1. A. Abbott, *Nature*, 2003, 424, 870–2.
2. V. M. Weaver, *J. Cell Biol.*, 1997, 137, 231–245.
3. P. A. Kenny, G. Y. Lee, C. A. Myers, R. M. Neve, J.R. Semeiks, P. T. Spellman, K. Lorenz, E. H. Lee, M. H. Barcellos-Hoff, O. W. Petersen, J. W. Gray and M. J. Bissell, *Mol. Oncol.*, 2007, 1, 84–96.
4. B. Weigelt and M. J. Bissell, *Semin. Cancer Biol.*, 2008, 18, 311–21.
5. D. Huh, G. A. Hamilton and D. E. Ingber, *Trends Cell Biol.*, 2011, 21, 745–54.
6. S. Chung, R. Sudo, P. J. Mack, C.-R. Wan, V. Vickerman and R. D. Kamm, *Lab Chip*, 2009, 9, 269–75.
7. K. Domansky, W. Inman, J. Serdy, A. Dash, M. H. M. Lim and L. G. Griffith, *Lab Chip*, 2010, 10, 51–8.
8. V. N. Goral, Y.-C. Hsieh, O. N. Petzold, J. S. Clark, P. K. Yuen and R. A. Faris, *Lab Chip*, 2010, 10, 3380–3386.
9. Y. Nakao, H. Kimura, Y. Sakai and T. Fujii, *Biomicrofluidics*, 2011, 5, 22212.
10. P. J. Lee, P. J. Hung and L. P. Lee, *Biotechnol. Bioeng.*, 2007, 97, 1340–6.
11. Y. Hsu, M. Moya, C. Hughes, S. George and A. Lee, in *MicroTAS 2011*, 2011, vol. 1, pp. 1382–1384.
12. K.-J. Jang and K.-Y. Suh, *Lab Chip*, 2010, 10, 36–42.
13. K.-J. Jang, H. S. Cho, D. H. Kang, W. G. Bae, T.-H. Kwon and K.-Y. Suh, *Integr. Biol.*, 2011, 3, 134–41.
14. H. J. Kim, D. Huh, G. Hamilton and D. E. Ingber, *Lab Chip*, 2012, 12, 2165–74.
15. J. H. Sung, J. Yu, D. Luo, M. L. Shuler and J. C. March, *Lab Chip*, 2011, 11, 389–92.
16. N. J. Douville, P. Zamankhan, Y.-C. Tung, R. Li, B. L. Vaughan, C.-F. Tai, J. White, P. J. Christensen, J. B. Grotberg and S. Takayama, *Lab Chip*, 2011, 11, 609–19.
17. D. Huh, B. D. Matthews, A. Mammoto, M. Montoya-Zavala, H. Y. Hsin and D. E. Ingber, *Science*, 2010, 328, 1662–8.
18. C. M. Puleo, W. McIntosh Ambrose, T. Takezawa, J. Elisseeff and T.-H. Wang, *Lab Chip*, 2009, 9, 3221–7.
19. A. Grosberg, P. W. Alford, M. L. McCain and K. K. Parker, *Lab Chip*, 2011, 11, 4165–73.
20. M. M. G. Grafton, L. Wang, P.-A. Vidi, J. Leary and S. Lelièvre, *Integr. Biol.*, 2011, 3, 451–459.
21. K. E. Sung, N. Yang, C. Pehlke, P. J. Keely, K. W. Eliceiri, Friedl and D. J. Beebe, *Integr. Biol.*, 2011, 3, 439–50.
22. J.-M. Peyrin, B. Deleglise, L. Saias, M. Vignes, P. Gougis, S. Magnifico, S. Betuing, M. Pietri, J. Caboche, P. Vanhoutte, J.-L. Viovy and B. Brugg, *Lab Chip*, 2011, 11, 3663–73.
23. D. Majumdar, Y. Gao, D. Li and D. J. Webb, *J. Neurosci. Methods*, 2011, 196, 38–44.
24. J. W. Song and L. L. Munn, *Proc. Natl. Acad. Sci. U. S. A.*, 2011, 108, 15342–7.
25. J. H. Sung and M. L. Shuler, *Lab Chip*, 2009, 9, 1385–94.
26. J. H. Sung, C. Kam and M. L. Shuler, *Lab Chip*, 2010, 10, 446–55.
27. Y. Imura, K. Sato and E. Yoshimura, *Anal. Chem.*, 2010, 82, 9983–8.

28. E. Westein, A. D. van der Meer, M. J. E. Kuijpers, J.-P. Frimat, A. van den Berg and J. W. M. Heemskerk, *Proc. Natl. Acad. Sci. U. S. A.*, 2013, 110, 1357–1362.
29. J. W. Song, S. P. Cavnar, A. C. Walker, K. E. Luker, M. Gupta, Y.-C. Tung, G. D. Luker and S. Takayama, *PLoS One*, 2009, 4, e5756.
30. D. Huh, D. C. Leslie, B. D. Matthews, J. P. Fraser, S. Jurek, G. A. Hamilton, K. S. Thorneloe, M. A. McAlexander and D. E. Ingber, *Sci. Transl. Med.*, 2012, 4, 159ra147–159ra147.
31. W.-M. Hsu, A. Carraro, K. M. Kulig, M. L. Miller, M. Kaazempur-Mofrad, E. Weinberg, F. Entabi, H. Albadawi, M. T. Watkins, J. T. Borenstein, J. P. Vacanti and C. Neville, *Ann. Surg.*, 2010, 252, 351–7.
32. A. Carraro, W.-M. Hsu, K. M. Kulig, W. S. Cheung, M. L. Miller, E. J. Weinberg, E. F. Swart, M. Kaazempur, Mofrad, J. T. Borenstein, J. P. Vacanti and C. Neville, *Biomed. Microdevices*, 2008, 10, 795–805.
33. A. Zijlstra, D. J. Webb and D. Li, *Biomed. Microdevices*, 2011, 13, 539–48.
34. H. Ma, T. Liu, J. Qin and B. Lin, *Electrophoresis*, 2010, 31, 1599–605.
35. S.-Y. C. Chen, P. J. Hung and P. J. Lee, *Biomed. Microdevices*, 2011, 13, 753–8.
36. S. Podszun, P. Vulto, H. Heinz, S. Hakenberg, C. Hermann, T. Hankemeier and G. A. Urban, *Lab Chip*, 2012, 12, 451–7.
37. D. Puchberger-Enengl, S. Podszun, H. Heinz, C. Hermann, P. Vulto and G. A. Urban, *Biomicrofluidics*, 2011, 5, 44111–4411110.
38. P. Vulto, G. Dame, U. Maier, S. Makohliso, S. Podszun, P. Zahn and G. A. Urban, *Lab Chip*, 2010, 10, 610–6.
39. P. Vulto, S. Podszun, P. Meyer, C. Hermann, A. Manz and G. A. Urban, *Lab Chip*, 2011, 11, 1596–1602.
40. P. Vulto, G. Medoro, L. Altomare, G. A. Urban, M. Tartagni,
41. R. Guerrieri and N. Manaresi, *J. Micromech. Microeng.*, 2006, 16, 1847–1853.
42. P. Vulto, N. Glade, L. Altomare, J. Bablet, L. Del Tin,
43. G. Medoro, I. Chartier, N. Manaresi, M. Tartagni and
44. R. Guerrieri, *Lab Chip*, 2005, 5, 158–62.
45. P. Vulto, T. Huesgen, B. Albrecht and G. A. Urban, *J. Micromech. Microeng.*, 2009, 19, 077001
46. T. Huesgen, G. Lenk, B. Albrecht, P. Vulto, T. Lemke and
47. P. Woias, *Sens. Actuators, A*, 2010, 162, 137–144.
48. K. Wrzesinski and S. J. Fey, *Toxicol. Res.*, 2013, 2, 123.
49. S. Ramaiahgari, M. Den Beaver, B. Herpers, J. N.
50. M. Commandeur, B. van de Water and L. Price, 2013, submitted.
51. S. J. Fey and K. Wrzesinski, *Toxicol. Sci.*, 2012, 127, 403–11.



